A Numerical Model for Evolution of Internal Structure of Cloud Cavitation

Tezhuan Du[1]*, Chenguang Huang[1], Yiwei Wang[1]

ISROMAC 2016

International Symposium on Transport Phenomena and Dynamics of Rotating Machinery

Hawaii, Honolulu

April 10-15, 2016

Abstract

Interaction between bubbles in cloud cavitation play an important role in cavitating flows. A numerical model was developed to study the internal structure and collapse of cloud cavitation. The model consists of : (1) an evolution model of bubble number density taking bubble breakup effects into account; (2) a modified cavitation model based on dynamics of bubble cluster; and (3) the multi-phase Reynolds Averaged Navier-Stokes equations (RANS) for background flow. The evolution model of bubble number density is governed by a transport type equation and the expression of source term is derived from a bubble breakup model. The condensation rate is constructed through dimension analysis and direct simulation of collapse of bubble cluster. The proposed model was tested by flows over a projectile. The results show that the evolution of internal structure of the cloud cavitation is closely related to the development of re-entrant jet. Moreover, the performance of proposed model and the effects of bubble number density on cavitating flows are discussed.

Keywords

cloud cavitation —bubble number density —bubble breakup—bubble cluster

[1]*Institute of Mechanics, Chinese Academy of Sciences, Beijing, 100190, China*

***Corresponding author**: dutezhuan@imech.ac.cn

INTRODUCTION

Cavitation is the key issue in the high-speed underwater propulsion, which can result in structure failure and acoustic. Cloud cavitation, as one of the most common type of cavitation for the marine vessels and projectile, is consists of a large amount of small bubbles. The pressure pulse generated by the bubble collapse in the cloud cavitation is usually considered to be the major cause of the structure failure and the noise radiation.

Numerical simulations are commonly used to study cavitating flows in many applications, such as hydrofoils, projectiles, and turbo machines, etc. Most of the researches were focused on the homogeneous flow modelling which is based on the Navier-Stokes equations of mixture phase. Kubota [1] , Merkle [2], Kunz [3] and Singhal [4] proposed a number of cavitation models based on the phase-change method respectively. However, the limitation of the homogeneous cavitation modeling is apparent, since it is only capable of providing macro-solutions of vapor volume fraction while the micro mechanism of cavitation evolution remains unknown. The evolution of the cloud cavitation includes various micro-physical processes such as the bubble collapse and the development of the re-entrant jet, and is highly related to the distribution of bubbles in terms of the size and number. For example, bubble clusters with different distributions may lead to different collapse pressures due to the interaction of bubbles while the vapor volume fractions can be identical. Therefore, the numerical model taking account of the internal structure of cloud cavitation will be essential for the understanding of the bubble evolution, and is expected to improve the prediction of the bubble collapse pressure.

Similar considerations of modeling small particle distributions can be found in many chemical engineering simulations. A statistical model of the dispersed phase is usually adopted in dispersed flows to describe the distribution of particle size [6]-[9], in which the evolution of the distribution function is governed by a Boltzmann-type equation. Unlike the chemical engineering applications, in which most of the models were based on the steady state condition and fully developed homogeneous turbulence, the cavitating flows with the evolution of cloud cavitation are highly unsteady and far more complex in terms of the flow physics.

In the present paper, the evolution model of bubble number density is proposed to simulate the process of the bubble breakup and transportation. A condensation rate based on bubble cluster is deduced by dimensional analysis and direct simulation. A numerical strategy is established to solve the flow with cloud cavitation combining our model with the homogeneous cavitation model, and was applied to the simulation of the cavitating flow around a projectile. The solutions can predict the evolution of both the outline and the internal structure of the cloud cavitation, which are in good agreement with the experimental observations.

1. Evolution model of the bubble number density

The original homogeneous cavitation models can provide the vapor volume fraction only, but the information of the internal structure of the cloud cavitation such as the bubble number density and the averaged bubble size remains

unknown. In the present work, we introduce a new transport equation of the bubble number density to the homogeneous cavitation model, so that the internal structure of cavitation can be solved. The transport equation of the bubble number density can be constructed as follows

$$\frac{\partial}{\partial t}(\rho_m n) + \nabla\bullet(\rho_m \vec{u} n) = S_n \tag{1}$$

where

$\rho_m = \alpha_v \rho_v + (1-\alpha_v)\rho_l$ denotes the density of mixture phase.

$\vec{u}_m = \frac{\alpha_l \rho_l \vec{u}_l + \alpha_v \rho_v \vec{u}_v}{\rho_m}$ represents the averaged velocity of mixture phase.

S_n is the source term involving the bubble breakup and coalescence. In the present work, only the effect of bubble breakup is taken into account.

Cavitation cloud is normally a bubble cluster which consists of large amounts of small bubbles with various sizes. Bubble-bubble interaction plays an essential role in the collapse of the bubble cluster, and will become stronger while the bubble cluster gets more compact. Given a homogeneous bubble cluster, the vapor volume fraction α can be related to the bubble number density n and the averaged bubble size $\bar{r}$ as:

$$\alpha = \frac{4}{3} n \pi \bar{r}^3 \tag{2}$$

Assuming the vapor volume fraction being constant in the process of bubble breakup, the source term of Eq. (1) can be written as follows：

$$S_n = -\frac{9\rho_m \alpha}{4\pi \bar{r}^4}\frac{\partial \bar{r}}{\partial t} \tag{3}$$

The averaged bubble size is given by:

$$\bar{r} = \int_0^\infty f(t,r) r dr \tag{4}$$

where $f(t,r)$ is the probability density function of bubble size at time t.

1.1 Bubble breakup model

Bubbles break up in turbulent flows when the velocity of turbulent fluctuations exceeds a threshold value. In other word, the bubble breaks up in turbulent flows when the bubble size exceeds a critical value, which is related to the turbulent fluctuations and the surface tension. Refer to Sosinovich [10], the evolution equation of probability density function of bubble size can be written as:

$$\frac{\partial f(t,r)}{\partial t} = -\int_0^r \frac{f(t,r)}{\tau(r)}\omega(\eta_1, r)d\eta_1 + \int_r^\infty \frac{f(t,R)}{\tau(R)}\omega(r,R)dR \tag{5}$$

where $\tau(r)$ represents the breakup time of a bubble of radius r, and the breakup function $\omega(r,R)$ represents the probability of a bubble of size R breaking into bubbles of size r. Neglecting the convection effect, the effects of bubble breakup on the time rate of probability density function can be divided into two parts: The first term on right hand side of Eq. (5) represents the decrease in probability function due to the bubbles of size r breaking into smaller ones, the second term indicates the increase in probability function due to bubbles of radii $r_1 > r$ break into ones of size r.

It is known that a bubble will break into two bubbles near the critical Weber number[11], based on which the breakup function can be given as follows:

$$\omega(r,R) = \theta(R-r)\theta(R-a_{cr})\delta\left(r - \frac{R}{\sqrt[3]{2}}\right) \tag{6}$$

where $\theta(x)$ is the step function, and a_{cr} is the critical size, which is determined by the following equation [11]:

$$\int_0^{2a_{cr}} P(t,r)dr = (1/C_f)^{1/3}(\sigma/\rho_l)(\rho_l/\rho_a)^{1/3} \tag{7}$$

where $C_f = 0.5$ is drag coefficient of a spherical bubble, $\sigma = 0.074$ is surface tension, ρ_l and ρ_a denote density of liquid and gas, respectively. $P(t,r)$ is the turbulent kinetic energy distribution over length scales, which can be expressed as follows：

$$P(t,r) = \frac{k}{\sqrt{2\pi}\sigma_p}\exp\left[\frac{-1}{2\sigma_p^2}(r-L)^2\right] \tag{8}$$

where $L = C_\mu \frac{k^{3/2}}{\varepsilon}$ is the turbulence length scale which describes the size of large energy-containing eddies in turbulent flows. k is the turbulent kinetic energy, and ε is the turbulent dissipation rate. $C_\mu = 0.1$ is a constant, and $\sigma_p = 0.005$ represents the standard error.

The bubble breakup time τ is the key parameter in the bubble breakup model, which determines the speed of the bubble breakup process. Assuming that a bubble breakup along the midsection into two bubbles, the breakup time can be written as :

$$\tau(r) = a_t \frac{r}{\sqrt{k}} \tag{9}$$

Considering that surface tension will impede the process of bubble breakup, an additional term $a_t b_t \frac{1}{\sqrt{k}r}$ is introduced to model the effect of surface tension and avoid divergence near r =0. So the breakup duration can be modeled as follows:

$$\tau(r) = a_t \frac{1}{\sqrt{k}}\left(r + b_t \frac{1}{r}\right) \tag{10}$$

where r and $\sqrt{k}$ represent the characteristic length and characteristic velocity, respectively. a_t and b_t are case dependent user defined constants . $a_t = 5\times10^{-4}$ and $b_t = 10^{-6}$ are suitable for this model.

substituting Eq.(6) into Eq.(5) we obtain :

$$\frac{\partial f(t,r)}{\partial t}=-\frac{f(t,r)}{\tau(r)}\theta\left(r-a_{cr}(t)\right)+\frac{f(t,\sqrt[3]{2}r)}{\tau(\sqrt[3]{2}r)}\theta\left(\sqrt[3]{2}r-a_{cr}(t)\right) \tag{11}$$

Using Eqs. (4), (10), we can derive the evolution equation of the averaged bubble size:

$$\frac{\partial \bar{r}}{\partial t}=\int_0^{\infty}\left[-\frac{f(t,r)}{\tau(r)}\theta\left(r-a_{cr}(t)\right)+\frac{f(t,\sqrt[3]{2}r)}{\tau(\sqrt[3]{2}r)}\theta\left(\sqrt[3]{2}r-a_{cr}(t)\right)\right]rdr \tag{12}$$

where

$$\int_0^{\infty}\left[-\frac{f(t,r)}{\tau(r)}\theta\left(r-a_{cr}(t)\right)\right]rdr=-\int_{a_{cr}}^{\infty}\frac{f(t,r)}{\tau(r)}rdr \tag{13}$$

$$\int_0^{\infty}\left[\frac{f(t,\sqrt[3]{2}r)}{\tau(\sqrt[3]{2}r)}\theta\left(\sqrt[3]{2}r-a_{cr}(t)\right)\right]rdr=\frac{1}{\sqrt[3]{4}}\int_{a_{cr}}^{\infty}\frac{f(t,r)}{\tau(r)}rdr \tag{14}$$

Thus Eq. (11) can be rearranged as follows：

$$\frac{\partial \bar{r}}{\partial t}=\left(\frac{1}{\sqrt[3]{4}}-1\right)\int_{a_{cr}}^{\infty}\frac{f(t,r)}{\tau(r)}rdr \tag{15}$$

substituting Eqs. (14) and (4) into Eq.(3) we obtain the source term in the transport equation of the bubble number density:

$$S_n=-\frac{9\rho_m\alpha}{4\pi}\left[\int_0^{\infty}f(t,r)rdr\right]^{-4}\left[\left(\frac{1}{\sqrt[3]{4}}-1\right)\int_{a_{cr}}^{\infty}\frac{f(t,r)}{\tau(r)}rdr\right] \tag{16}$$

During the simulation, the probability density function of bubble size is given by:

$$f(t,r)=\frac{1}{\sqrt{2\pi}\sigma_f}\exp\left[\frac{-1}{2\sigma_f^2}\left(r-\sqrt[3]{\alpha\Big/\frac{4}{3}\pi n}\right)^2\right] \tag{17}$$

where σ_f is the standard error and set to be $\sigma_f=0.3\bar{r}$.

The evolution of the bubble number density can be simulated by solving Eqs. (1), (16).

2. Condensation rate based on bubble cluster

In the present work, we are focusing on the bubble-bubble interaction in the collapse stage of cavitation cloud. A condensation rate based on bubble cluster will be constructed in this section.

2.1 Dimension analysis of collapse of bubble cluster

Consider a bubble cluster collapsing under pressure p_∞ (Figure 1). Assuming that all bubbles are spherical and in the state of equilibrium at the beginning.

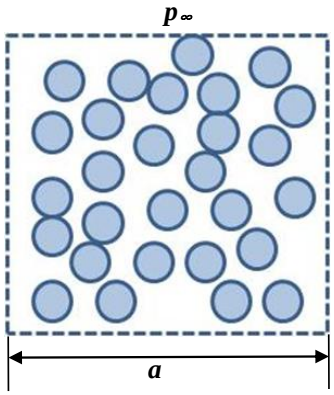

Figure 1 Schematic of bubble cluster

The related parameters are listed as followed:

Time: $t[T]$;

Characteristic length of bubble cluster: $a[L]$;

Initial bubble radii: $R_0[L]$;

Population of bubbles per unit volume: $n[\frac{1}{L^3}]$;

Material parameters: liquid density $\rho_L[\frac{M}{L^3}]$, liquid viscosity $\mu_L[\frac{M}{LT}]$, surface tension $S[\frac{M}{T^2}]$, reference density of gas $\rho_{A0}[\frac{M}{L^3}]$, gas viscosity $\mu_A[\frac{M}{LT}]$, ratio of specific heats of gas $\gamma[1]$;

Surrounding pressure $p_\infty[\frac{M}{LT^2}]$, pressure inside bubbles $p_B[\frac{M}{LT^2}]$;

The variation rate of volume of all bubbles can be expressed in a relationship:

$$\dot{V}=f(t;R_0,a;n;\rho_L,\mu_L,S,\rho_{A0},\mu_A,\gamma;p_\infty,p_B) \tag{18}$$

Taking t, R_0, ρ_L as a unit system produces dimensionless form:

$$\frac{\dot{V}}{\frac{4}{3}\pi R_0^3\Big/t}=f\left(\frac{a}{R_0};nR_0^3;\frac{\mu_L}{\rho_L R_0^2\Big/t},\frac{S}{\rho_L R_0^3\Big/t^2},\right. \tag{19}$$

$$\left.\frac{\rho_{A0}}{\rho_L},\frac{\mu_A}{\rho_L R_0^2\Big/t},\gamma,\frac{p_\infty}{\rho_L R_0^2\Big/t^2},\frac{p_\infty-p_B}{\rho_L R_0^2\Big/t^2}\right)$$

where $\frac{a}{R_0}$ can be rewritten as population of bubbles $N=\frac{a^3}{R_0^3}(nR_0^3)=a^3n$, and nR_0^3 can be converted to void fraction $\alpha=n\frac{4}{3}\pi R_0^3$. Taking collapse time of single bubble $T_C=0.915R_0\sqrt{\frac{\rho_L}{p_\infty-p_B}}$ as characteristic time, the relationship becomes:

$$\frac{\dot{V}}{\frac{4}{3}\pi R_0^3/T_C} = f(\alpha; N; \frac{\mu_L}{\rho_L R_0^2/T_C}, \frac{S}{\rho_L R_0^3/T_C^2}, \frac{\rho_{A0}}{\rho_L}, \frac{\mu_A}{\rho_L R_0^2/T_C}, \gamma, \frac{p_\infty}{p_\infty - p_B}, \frac{t^2}{T_C^2}) \quad (20)$$

The collapse of bubbles is controlled by pressure difference and inertial force, so viscosity and surface tension can be neglected. For given material $\frac{\rho_{A0}}{\rho_L}$ and γ are constant. Thus, Equation can be reduced to:

$$\frac{\dot{V}}{\frac{4}{3}\pi R_0^3/T_C} = f(\alpha; N; \frac{p_\infty}{p_\infty - p_B}, \frac{t^2}{T_C^2}) \quad (21)$$

In Eq.(21) $\frac{p_\infty}{p_\infty - p_B}$ can be replaced by $p' = \frac{p_\infty - p_B}{p_\infty}$ which represents non-dimensional driving pressure. Consider average variation rate of volume, the non-dimensional time will not appear in the formulation:

$$\frac{\dot{V}}{\frac{4}{3}\pi R_0^3/T_C} = f(\alpha; N; p') \quad (22)$$

where $\dot{v}_0 = \frac{4}{3}\pi R_0^3/T_C$ represents volume variation rate of single bubble, therefore $\dot{V}' = \dot{V}/\dot{V}_0$ is non-dimensional volume variation rate of bubble cluster. We can see from the Eq. (22) that three key parameters: α, N and p' ,To provide the specific relation, we can assume that:

$$\dot{V}' = c\alpha^{k_1} N^{k_2} p'^{k_3} \quad (23)$$

The empirical parameters c, k_1, k_2, k_3 can be determined by direct simulation of collapse of bubble clusters.

2.2 Direct simulation of collapse of bubble cluster

Consider a cubic bubble cluster in which bubbles are arranged in $n \times n \times n$ order as shown in Figure 2. The initial pressure inside bubble cluster is set to be p_B, and the pressure at boundary is p_∞.

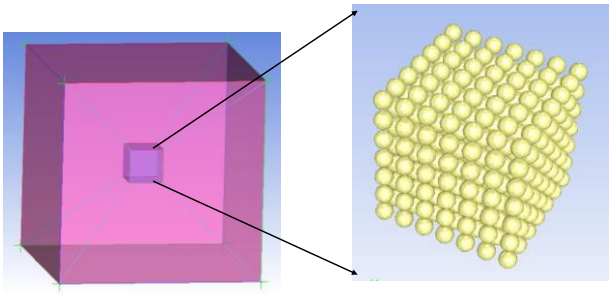

Figure 2 Flow field and numerical model

Volume of fraction (VOF) method and large eddy simulation (LES) are adopted in the numerical simulations. The parameters are listed as follows:

Volume faction α: 0.150, 0.268, 0.500

Population of bubbles N: 3^3, 4^3, 5^3, 6^3

Non-dimensional pressure p':0.6, 0.7, 0.8, 0.9

The volume variation rate of bubble cluster is recorded during the calculation and averaged by time. The following discussions are carried out around non-dimensional time-averaged volume variation rate.

2.2.1. Influence of bubble population

Table 1~ Table 3 give the $\dot{V}'$ under different bubble populations, where R_B represents initial bubble radii, D_B is the distance between the centers of two neighbor bubbles.

Table 1. $\dot{V}'$ corresponding to different bubble populations (α=0.150)

Parameters	1	2	3	4
N	3×3×3	4×4×4	5×5×5	6×6×6
R_B (mm)	6.87	5.15	4.12	3.43
D_B (mm)	20.8	15.6	12.5	10.4
$\dot{V}'$	-10.7	-19.6	-31.4	-45.6

Table 2. $\dot{V}'$ corresponding to different bubble populations (α=0.268)

Parameters	1	2	3	4
n	3×3×3	4×4×4	5×5×5	6×6×6
R_B（mm）	8.33	6.25	5 .00	4.16
D_B（mm）	20.8	15.6	12.5	10.4
$\dot{V}'$	-9.97	-18.2	-29.0	-42.1

Table 3. $\dot{V}'$ corresponding to different bubble populations（α=0.500）

Parameters	1	2	3	4
n	3×3×3	4×4×4	5×5×5	6×6×6
R_B（mm）	10.3	7.69	6.15	5.13
D_B（mm）	20.8	15.6	12.5	10.4
$\dot{V}'$	-9.05	-16.4	-25.9	-37.3

Curve fitting gives the power-law exponent k_2=0.68 .The power-law exponent of bubble population is close to $2/3$. It's because bubble cluster is collapsing approximately layer by layer (Figure 3), and the number of bubbles outer is of the order $O(N^{2/3})$.

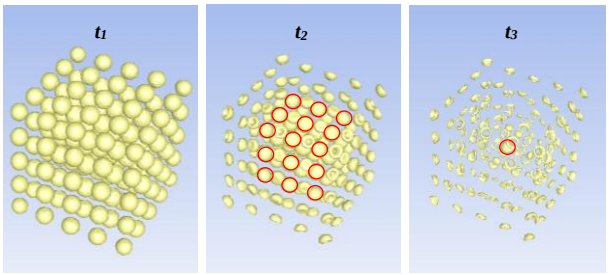

Figure 3 Collapse of bubble cluster (α =0.150, N=5^3, p' =0.8)

2.2.2. Influence of volume fraction

Similarly, we can provide the power-law exponent of α using the data of Table 4

Table 4. $\dot{V}'$ corresponding to different volume fractions

α \ N	3×3×3	4×4×4	5×5×5	6×6×6
0.15	-10.7	-19.6	-31.4	-45.6
0.268	-9.97	-18.2	-29.0	-42.1
0.5	-9.05	-16.4	-25.9	-37.3

Curve fitting shows that the power-law exponent of α is k_1=–0.160. Higher α corresponds to a compacter bubble cluster. Therefore, the inner bubbles will reduce the collapse velocity of outer bubbles. On the contrary, the outer layer of bubbles will shield the inner bubbles from collapsing. As a result, the collapsing velocity will slow down with the rise of volume fraction.

2.2.3. Influence of non-dimensional pressure

Non-dimensional pressure represents the driving force for collapse of bubble cluster. With the increase of p', the collapse will become more violent (Figure 4).

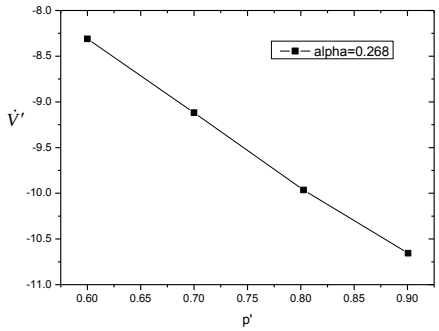

Figure 4 Curve of $\dot{V}'$ corresponding to p'

Curve fitting gives the power-law exponent k_3=0.609.

p' represents the driving pressure of collapse of bubble cluster. It affects not only the collapse velocity but also the procedure of collapse.

2.3 Condensation rate

The constant coefficient C is closed to 1, combined with the influence of α, N and p', Eq. (23) becomes:

$$\dot{V}'=\alpha^{-0.16}N^{0.69}p'^{0.61} \tag{24}$$

Equation (24) gives the no-dimensional collapse velocity of bubble cluster. Then the change rate of void fraction can be given as:

$$\dot{\alpha}=\frac{\dot{V}}{V_m}=-0.0039\alpha^{-0.2}N^{0.68}p'^{0.609}\frac{\frac{4}{3}\pi R_0^3}{V_m T_C} \tag{25}$$

The cavitation rate $\dot{m}$ is related to $\dot{\alpha}$ as [4]:

$$\dot{m}=\frac{\rho_l\rho_v}{\rho_m}\dot{\alpha} \tag{26}$$

substituting Equation (25) into Equation (26), we can get the condensation rate as follows:

$$\dot{m}^-=-C_c\frac{\rho_l\rho_v}{\rho_m}\left(\frac{n^{0.013}}{V_m^{0.32}\alpha^{0.533}}\right)\alpha\left(\frac{p-p_v}{p}\right)^{0.609}\sqrt{\frac{2(p-p_v)}{3\rho_l}} \tag{27}$$

where V_m is the volume of a mesh cell, and C_c=0.057.

According to Singhal model, the vaporation rate is set to be:

$$\dot{m}^+=C_e\rho_l\frac{\rho_l\rho_v}{\rho}\frac{\sqrt{k}}{\sigma}(1-\alpha-\alpha_g)\sqrt{\frac{2}{3}\frac{p_v-p}{\rho_l}} \tag{28}$$

3. Numerical strategy

The basic approach for cavitating flows consists of unsteady Reynolds Averaged Navier-Stokes equations of the mixture phase and the continuity equation of the vapor phase.

The numerical procedure of the cloud cavitation computation is demonstrated in Figure 5.

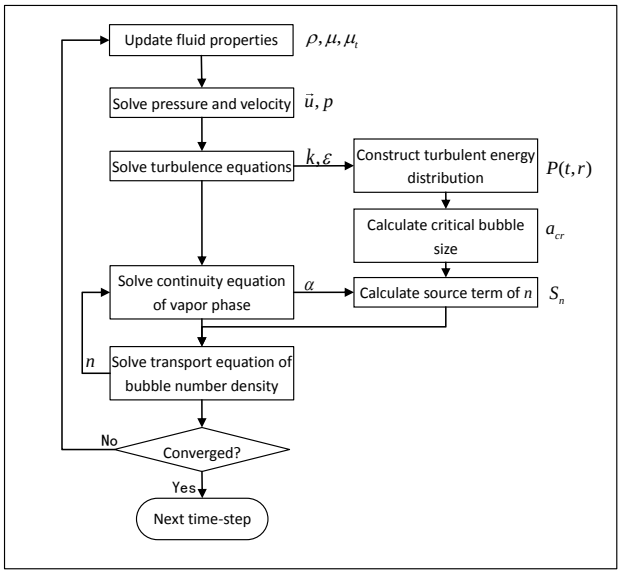

Figure 5 Numerical procedure.

Unsteady RANS equations combined with modified RNG k-ε model [12] are solved by FLUENT using SIMPLEC algorithm to provide background flow information to the continuity equation of vapor phase and transport equation of bubble number density, which are computed in sequence. The calculation of additional transport equation of bubble number density and its source term consumes more computing power, which depends on the mesh size and the resolution of the bubble size distribution function.

4. Validation

The simulation of the cavitating flow over a cylindrical body with 90° blunt conical head is presented in this section. The diameter of cylinder is d=37.5mm, and the free-stream velocity is v=18m/s. The corresponding cavitation number and Reynolds number are σ=0.612, Re=6.75×105, respectively. The 2-D axisymmetric geometry is utilized in the simulation, with a 350×150 structural mesh, depicted in Figure 6. The

heigh of first grid layer is 2×10^{-4} mm， which makes sure that the wall y^+ is of the order O(1). The numerical results are validated by the experimental data based on the Split Hopkins Pressure Bar (SHPB) launch system [13].

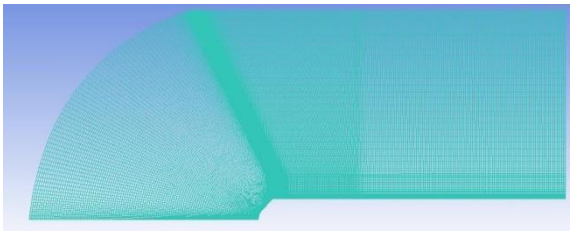

Figure 6 Computational domain.

Figure 7 ~ Figure 11 illustrate the evolution of the cloud cavitation. The yellow curves represent the iso-surface of vapor fraction with the value of 0.1, and the red zones in the cavitation indicate high bubble number density area ($n\geq10^9$) which can be seen as cloud cavitation.

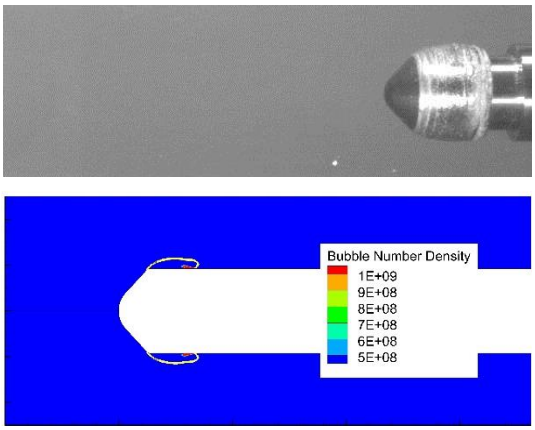

Figure 7 The growth of the sheet cavitation

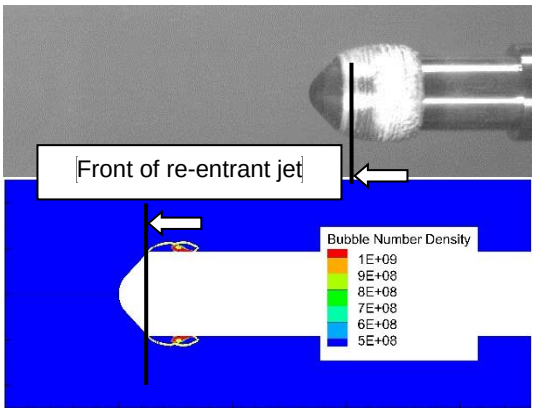

Figure 8 The development of the re-entrant jet.

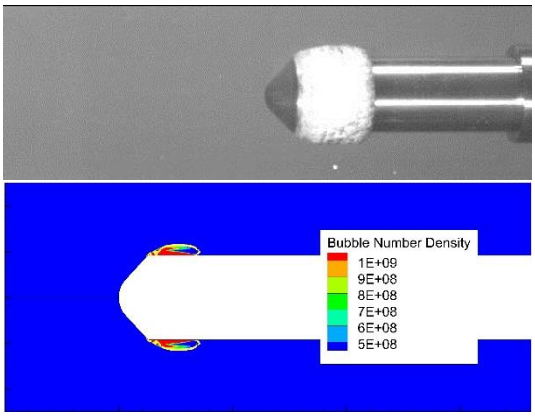

Figure 9 The full cloud cavitation.

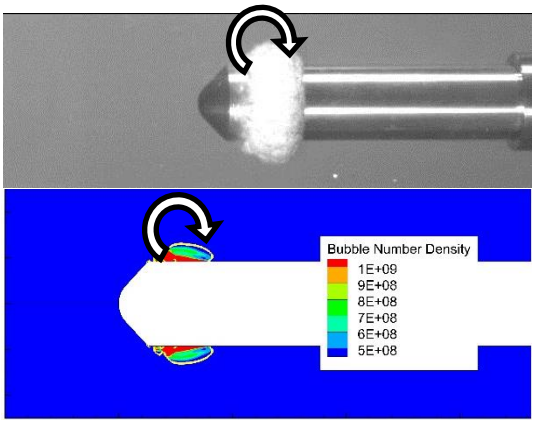

Figure 10 The detachment of cloud cavitation.

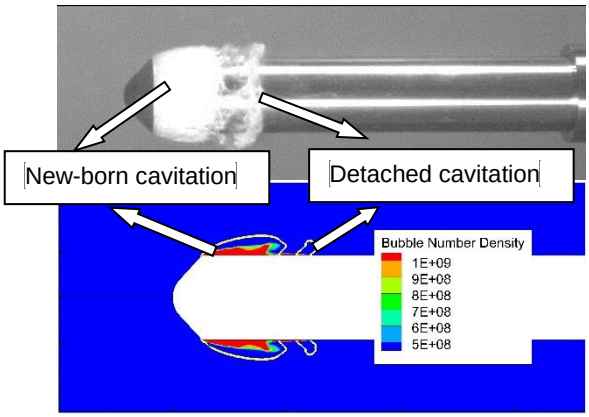

Figure 11 The collapse of the detached cavitation.

The evolution of cavitation can be divided into four stages: the growth of the sheet cavitation, the development of re-entrant jet, the detachment of cavitation cloud, and the collapse of detached cavitation cloud. When the cavitation occurs, a transparent laminar void like a flat bubble starts to grow from the shoulder of the projectile (Figure 7).

The bubbles then start to break up as the re-entrant jet develops, with a simultaneous increase of the bubble number density. The breakup process turns the sheet cavitation to the cloud cavitation (Figure 8).

The whole cavitation area turns into a non-transparent cavitation cloud when re-entrant jet reaches the shoulder of the projectile (Figure 9), where the cavitation cloud detaches and rolls downstream with the mean flow until collapse (Figure 10, Figure 11). Meanwhile, new attached cavitation appears at the shoulder of projectile. The simulation results show that the formation of cloud cavitation is closely related to the re-entrant jet.

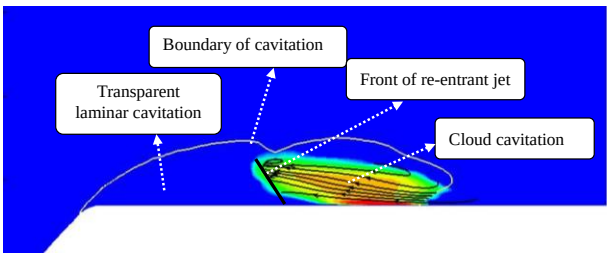

Figure 12 Formation of cloud cavitation

Figure 12 illustrates the outline of cavitation and the

distribution of bubble number density n. It can be seen that cloud cavitation area is consistent with the region swept by the re-entrant jet, which suggests that the re-entrant jet breaks bubbles into small ones, and forms the cavitation cloud.

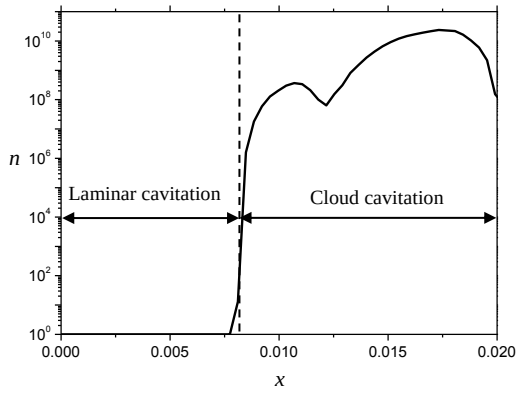

Figure 13 Distribution of the bubble number density in the cavitation.

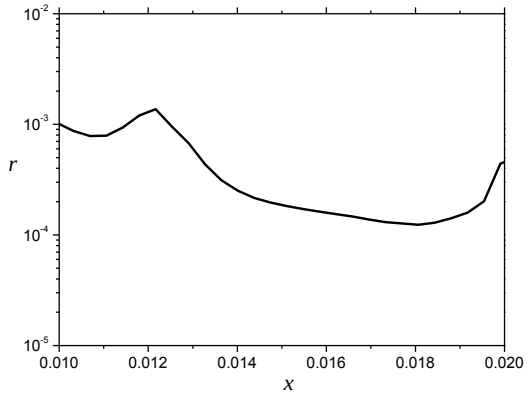

Figure 14 Distribution of the bubble size in the cavitation cloud.

Figure 13 presents the distribution of the bubble number density in the cavitation region along the wall of projectile, and the origin of X axis represents the leading edge of cavitation. The cavitation can be divided by re-entrant jet into two parts: the transparent laminar cavitation and the nontransparent cloud cavitation. It is shown that the bubble number density increases rapidly at the front of re-entrant jet and decreases close to the cavitation closure. Bubble size is not uniform in the region of the cloud cavitation (Figure 14), the minimum value of $\overline{r}$ is 0.202 mm, which corresponds to the maximum n of 3.06×10^{10}.

Good agreement with the experimental data suggests that our numerical strategy is capable of predicting the evolution of cavitation with high precision. In addition, the distribution of the bubble number density solved by the proposed model can help us better understand the internal structure of cloud cavitation.

5. Disscussions

The bubble number density plays an important role in cavitating flows, especially in collapse process of cavitation [14]-[16]. There is an important characteristic named geometry focusing of collapse pressure in the collapse process of bubble cluster. The pressure waves emitted by collapse bubbles will propagate inward which leads to a higher magnitude of collapse pressure [17]. In this paper, we compare the present model with Singhal model to test the ability of predicting pressure focusing effect.

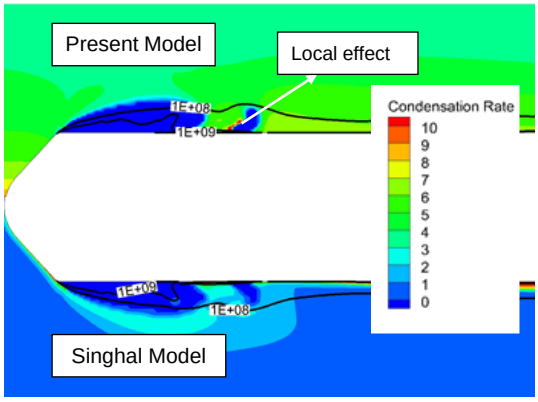

Figure 15 Comparation of condensation rates

Figure 15 shows that present model presents a higher condensation rate than Singhal model. That means present model will predict a higher collapse pressure thant Singhla model (Figure 16). Further more, the condensation rate of Singhal model is quit smooth while present model shows local effects of collapse. The region of cavitation cloud with higher bubble number density collapse more fiercely than other else.

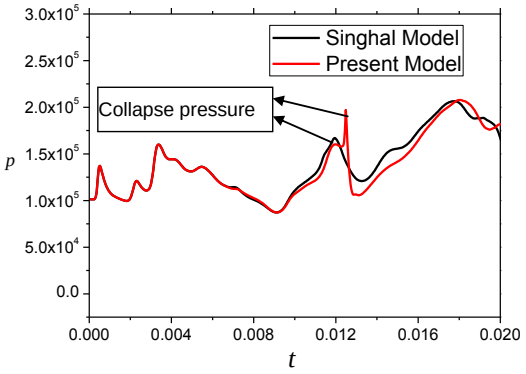

Figure 16 Comparation of collapse pressure (at x/d=2)

6. Conlusions

Homogeneous cavitation models can only give volume fractions of different phases. It's not enough for cavitating flow, especially for collapse of cloud cavitation. Different bubble sizes and bubble number density may be corresponding to the same vapor fraction. Cavitation cloud of different internal structure can result in different collapse pressure due to interaction between bubbles. Internal information of cloud cavitation is needed to predict collapse pressure more accurately.

In the present work, a numerical model consists of modified homogenous cavitation model and evolution equation of bubble number density was proposed. The evolution model of bubble number density is governed by a transport type equation and takes account of bubble breakup effect. The condensation rate is constructed through

dimension analysis and direct simulation of collapse of bubble cluster. This model was implemented on cavitating flow over a projectile with blunt conical head and validated by the experiment base on SHPB launch system. The simulation results showed that present model can predict the evolution of cavitation and the distribution of bubble number density (or bubble size) well.

The comparation of present model and Singhal modle was discussed. It is shown that the collapse pressure of detached cavitation cloud is strongly affected by bubble number density. Non-uniform distribution of bubble number density may lead to different collapse velocities. The region of cavitation cloud with higher bubble number density collapse more fiercely than other else.

The proposed model can solve the distribution of the bubble number density and help us better understand the internal structure of cloud cavitation. But, continuous efforts should be made to improve this model. First, only bubble breakup was considered in present model, the effects of coalescence needs to be studied. Second, although the breakup model is simplified, the present model is still time consuming. Further optimization for the numerical method is needed to enhance the computational efficiency.

REFERENCES

[1] A. Kubota, H. Kato, Unsteady structure measurement of cloud cavitation on a foil section, *Journal of Fluids Engineering*, 111(3):204~210, 1989.

[2] C. L. Merkle, J. Feng, P. E. O. Buelow, Computational modeling of the dynamics of sheet cavitation, *Proceedings of 3rd International Symposium on Cavitation*, Grenoble, France, 1998.

[3] R. F. Kunz, D. A. Boger, D. R. Stinebring, T. S. Chyczewski, J. W. Lindau, H. J. Gibeling, S. Venkateswaran, T. R. Govindan, A preconditioned Navier-Stokes method for two-phase flows with application to cavitation prediction, *Computers and Fluids*, 29(8): 849-875, 2000.

[4] A. K. Singhal, M. M. Athavale, H. Li, Y. Jiang, Mathematical Basis and Validation of the Full Cavitation Model, *Journal of Fluids Engineering*, 124(3): 617-624, 2002.

[5] J. C. Lasheras, C. Eastwood, C. Martínez-Bazán, J. L. Montañés, A review of statistical model for the break-up of an immiscible fluid immersed into a fully developed turbulent flow, *International Journal of Multiphase Flow*, 28: 247-278, 2002.

[6] C. Martínez-Bazán, J. L. Montañés, J. C. Lasheras, On the breakup of an air bubble injected into a fully developed turbulent flow. Part 1: Breakup frequency, *Journal of Fluid Mechanics*, 401: 157-182, 1999.

[7] C. Martínez-Bazán, J. L. Montañés, J. C. Lasheras, On the breakup of an air bubble injected into a fully developed turbulent flow. Part 2: Size pdf of the resulting daughter bubbles, *Journal of Fluid Mechanics*, 401: 183-207, 1999.

[8] G. M. Evans, P. M. Machniewski, A. K. Bin, Bubble size distribution and void faction in the wake region below a ventilated gas cavity in downward pipe flow, *Chemical Engineering Research and Design*, 82(A9):1095-1104, 2004.

[9] V. A. Sosinovich, V. A. Tsyganov, B. A. Kolovandin, B. I. Puris, V. A. Gertsovich, Modle of gas bubble breakup in turbulent liquid flow, *Journal of Engineering Physics and Thermophysics*, 68(2): 164-175, 1995.

[10] V. G. Levich, Physicochemical Hydrodynamics (English translation by Scripta Tchnica) [M], Prentice-Hall, Englewood Cliffs, USA, 1962.

[11] V. A. Sosinovich, V. A. Tsyganov, B. I. Puris, V. A. Gertsovich, Model of fractionation and coalescence of gas bubbles in a turbulent liquid flow, *Journal of Engineering Physics and Thermophysics*, 70(6): 918-926, 1997.

[12] J. L. Reboud, B. Stutz, O. Coutier, Two-phase flow structure of cavitation: experiment and modeling of unsteady effects, 3rd International Symposium on Cavitation, Grenoble, France, 1998.

[13] Y. P. Wei, Y. W. Wang, X. Fang, C. G. Huang, Z. P. Duan, A scaled underwater launch system accomplished by stress wave propagation technique, *Chinese Physics Letters*, 28(2): 024601, 2011.

[14] G. E. Reisman, C. E. Brennen, Shock wave measurements in cloud cavitation, *Proceedings of 21st International Symposium on Shock Waves*, Paper 1570, 1997.

[15] G. E. Reisman, Y. C. Wang, C. E. Brennen, Observations of shock waves in cloud cavitation, *Journal of Fluid Mechanics*, 355:255~283, 1998.

[16] L. Zhang, Z. Wen, X. Shao, Investigation of bubble-bubble interaction effect during the collapse of multi-bubble system, *Chinese Journal of Theoretical and Applied Mechanics*, 45(6): 861-867, 2013.

[17] Y. C. Wang, Distribution on the dynamics of a spherical cloud of cavitation bubbles, *Journal of Fluids Engineering*, 121:881~886, 1999.